Supporting Information

Zinc Triazolate Oxalate CALF-20 with Platelet Morphology and its PEBAX-based Mixed Matrix Membranes for CO$_2$/N$_2$ separation

Qian Jia,[a] Elsa Lasseuguette,[b] Harpreet Kaur,[a] Aaron B. Naden,[a] Maria-Chiara Ferrari[b*] and Paul A. Wright[a*]

[a] EaStCHEM School of Chemistry, University of St Andrews, Purdie Building, North Haugh, St Andrews KY16 9ST, U.K.

[b] School of Engineering, University of Edinburgh, Robert Stevenson Rd, Edinburgh EH9 3FB, U.K.

1. CALF-20 Synthesis and Characterisation

2. Preparation of PEBAX based MMMs and measurement of membrane performance

1. CALF-20 Synthesis and Characterisation

Chemical Reagents and Materials

PEBAX MH1657 (Arkema), zinc nitrate hexahydrate (Alfa Aesar, 98%), 1,2,4-triazole (thermos scientific, 99%), oxalic acid (Fisons, 99.8%), lithium hydroxide (Fisons), zinc carbonate basic (Glentham life science), Methanol (99.9%) and deionised (DI) water.

Literature Synthesis of CALF-20 and related

CALF-20 was synthesised by following the previously reported protocol.[1,2] 9 mmol oxalic acid dihydrate and 18 mmol 1,2,4-triazole were each dissolved in 5mL ethanol and DI water. The prepared solutions were combined and stirred for 1 h to give a cloudy white suspension. 17.5 mmol zinc carbonate basic was added to the mixture and stirred at room temperature for 24 h. The product was collected by filtration and washed with fresh ethanol three times. Additionally, a similar reaction mixture was heated for 1.5 at 90 °C in a microwave oven.

CALF-20 Platelet Synthesis

CALF-20 platelets were prepared by using zinc hydroxide nitrate as the precursor. Zinc hydroxy nitrate salt was synthesised by separately dissolving 2 mmol $Zn(NO_3)_2 \cdot 6H_2O$ and 1 mmol $Li(OH) \cdot H_2O$ in 10 mL DI water. After full dissolution, the basic solution was added dropwise into the zinc nitrate solution. The mixture was stirred for 30 min and subsequently filtered to collect the zinc hydroxy nitrate salt, which was identified from its PXRD pattern, measured in Bragg-Bentano geometry on a PAnalytical diffractometer (Cu $K_{\alpha1}$). At the same time, 16 mmol of 1,2,4-triazole and 1 mmol oxalic acid dihydrate were mixed in 20 mL methanol. The zinc hydroxide nitrate was added into the linker mixture. The resultant solution was transferred into 30 mL glass vessel for microwave synthesis and heated for 1.5 h at 90 °C. The product was collected and washed by centrifuge at 14500 rpm.

CALF-20 characterization

The crystalline structure of the as-synthesized CALF-20 was examined by powder X-ray diffraction (PXRD) in capillaries in Debye-Scherrer geometry on a Stoe STAD I/P diffractometer (Mo $K_{\alpha1}$ X-radiation, λ=0.7093 Å, 2θ range 1.5 - 27°). For visual comparison with most literature data, the experimental pattern was converted into that expected for Cu $K_{\alpha1}$ X-ray PXRD (λ = 1.54056 Å) by applying the equation:

$$\sin^{-1}\left(\frac{\sin\left(\frac{2\theta_{Mo}}{2}\right)}{0.460416}\right) \times 2 = 2\theta_{Cu}$$

(Eq. S2)

The morphology of CALF-20 was examined using electron microscopy (SEM) on a JSM-IT800 instrument. The image was imported into ImageJ to analyse the lateral dimensions of platelet CALF-20. Transmission electron microscopy (TEM) measurements were performed on an FEI Titan Themis operated at 200 kV, equipped with a 4k x 4k Ceta CMOS camera. The thickness of platelet CALF-20 were characterised by atomic force microscopy (AFM).

Functional groups were identified by using infrared spectroscopy (IR) on a Shimadzu IRAffinity 1S IR spectrometer.

Thermogravimetric analysis (TGA) was performed on a Stanton Redcroft STA-780 with a heating rate of 5 °C min^{-1}. N_2 adsorption isotherms were measured volumetrically using a Micrometrics ASAP 2020 Gas Adsorption Analyzer at 77 K. Before measurement, CALF-20 powder was activated in a tube furnace under N_2 at 423 K for 10 h. The activated samples were then evacuated at 423 K for 8 h to remove moisture. High-pressure N_2 and CO_2 uptake at 298 K was measured using a Hiden Intelligent Gravimetric Analyzer (IGA). The sample was activated at 423 K for 10 h prior to measurement. The activated samples were then heated under vacuum at the same temperature for 10 h. The mass change was recorded in each adsorption/desorption step, and each step stopped when the system has reached 98% of the asymptotic equilibrium value or after 90 min, whichever was shorter.
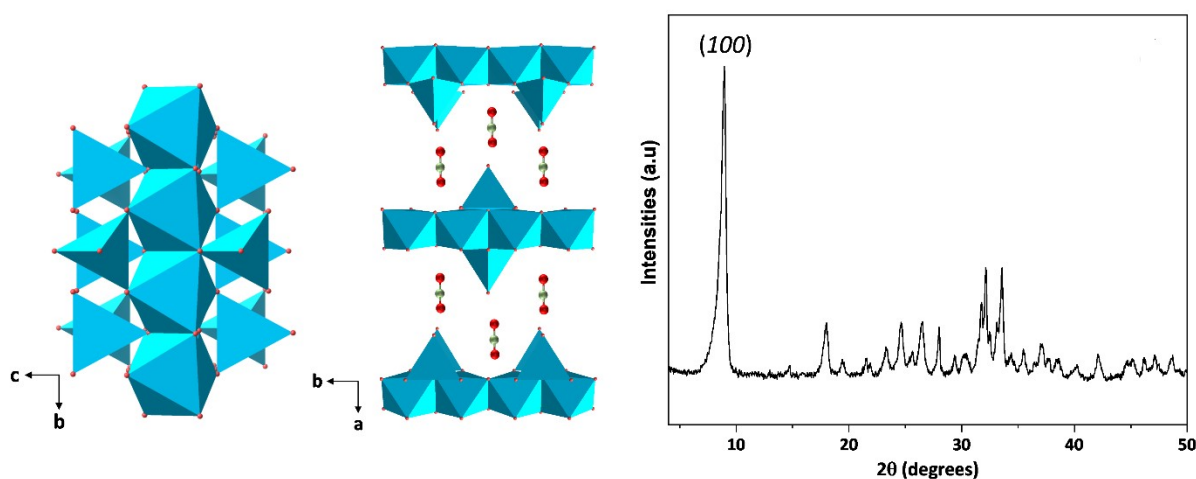

Figure S1. (Left) The layered structure of zinc hydroxy nitrate.[3] ZnO_4 tetrahedra and ZnO_6 octahedra in blue, nitrate anions in between layers. (Right) PXRD (Cu K$_\alpha$, 1.54056 Å) of zinc hydroxy nitrate.
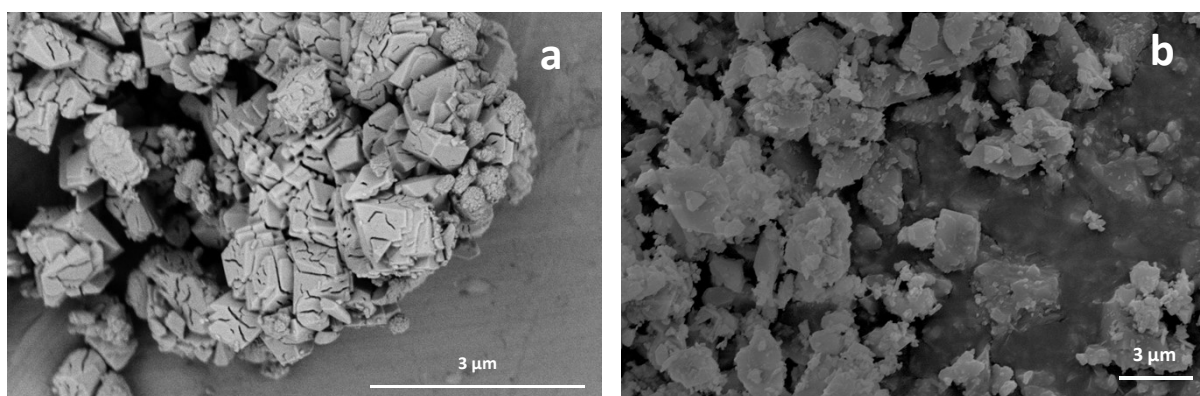
Figure S2. SEM image of CALF-20 synthesised by using zinc carbonate basic (a) at room temperature and (b) with microwave heating at 90 °C for 1.5 h.
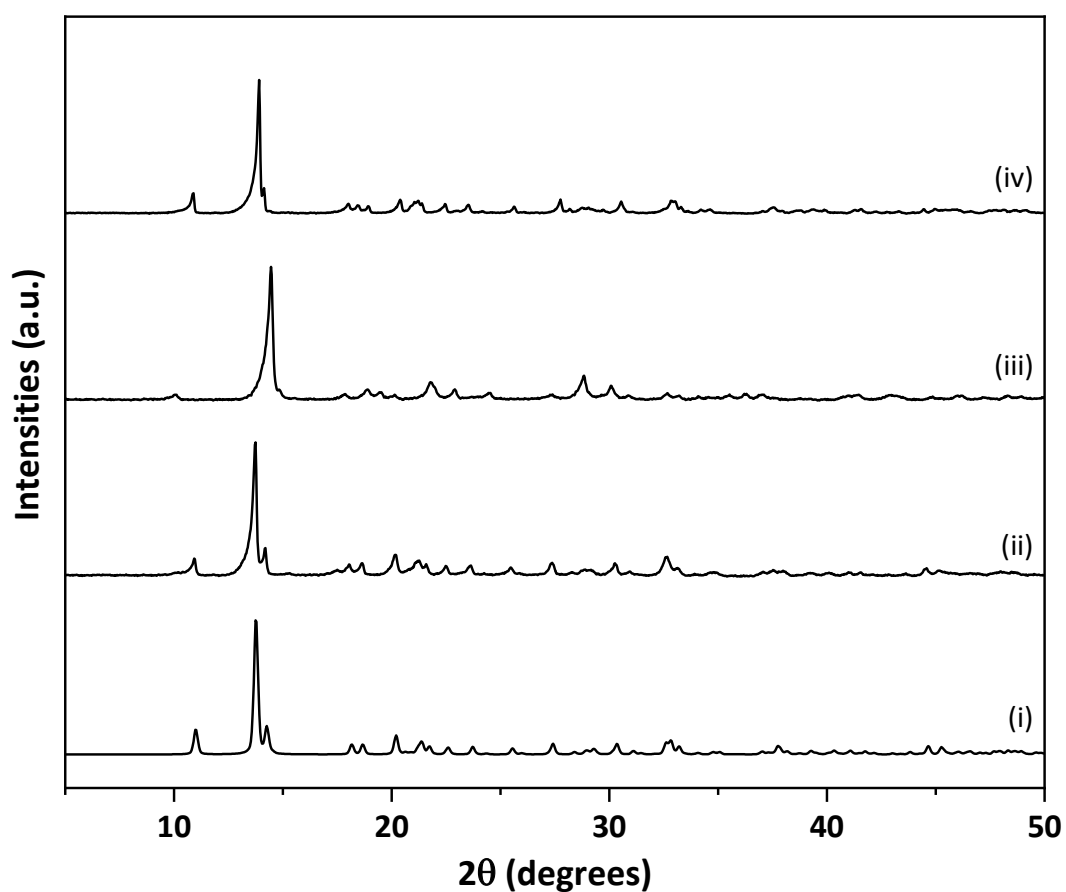

Figure S3. PXRD patterns (measured with Mo $K_{\alpha1}$ and represented as if from Cu $K_{\alpha1}$) of (i) simulated CALF-20(α), (ii) CALF-20 prepared according to the literature,[2] (iii) CALF-20 prepared with layered zinc hydroxide nitrate precursor with microwave heating and (iv) CALF-20 prepared using zinc carbonate basic with microwave heating. Only (iii) shows the PXRD pattern of CALF-20(β).
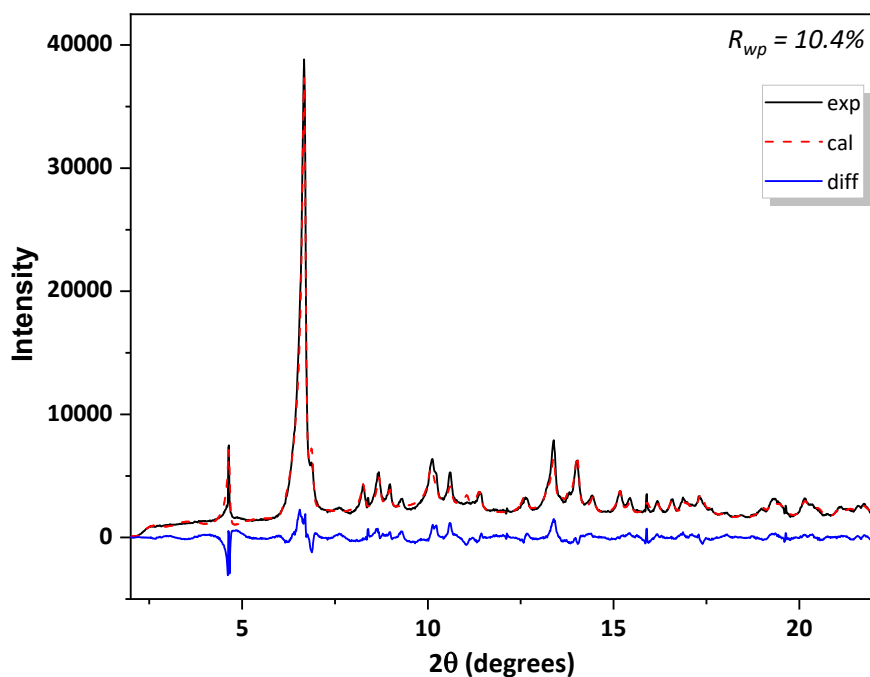
Figure S4. PXRD of CALF-20(β) (Mo K$_{\alpha1}$, λ = 0.7093 Å) matched by a refined structure: the black solid line represents experimental data; the red dash line represents the calculated data, and the blue solid line represents the difference between experimental and calculated data. The starting structure was adapted from that of a related material[4] and allowed to refine using rigid bodies for the oxalate and triazolate units.[5]

Table S1 Crystal data and structure refinement for CALF-20(P)

|						
program:						Topas
Crystal system, space group:						Monoclinic, *P2₁/c*
a, b, c :					9.3328(4) Å, 7.9980(4) Å, 9.9981(5) Å	
β:						110.878°
V(Å³):						697.295
R$_{wp:}$						10.40%
Site	**Type**	**x**	**y**	**z**	**Occ**	**Mult**
Zn1	Zn	0.3100	0.5400	0.5360	1.000	4
C1	C	0.3121	0.7503	0.2847	1.000	4
C2	C	0.5209	0.6986	0.2661	1.000	4
C4	C	0.0087	0.4193	0.5471	1.000	4
N1	N	0.3850	0.6529	0.3938	1.000	4
N2	N	0.3935	0.7821	0.2018	1.000	4
N3	N	0.5235	0.6179	0.3827	1.000	4
O1	O	0.1420	0.3739	0.6171	1.000	4
O2	O	-0.1095	0.3465	0.5467	1.000	4
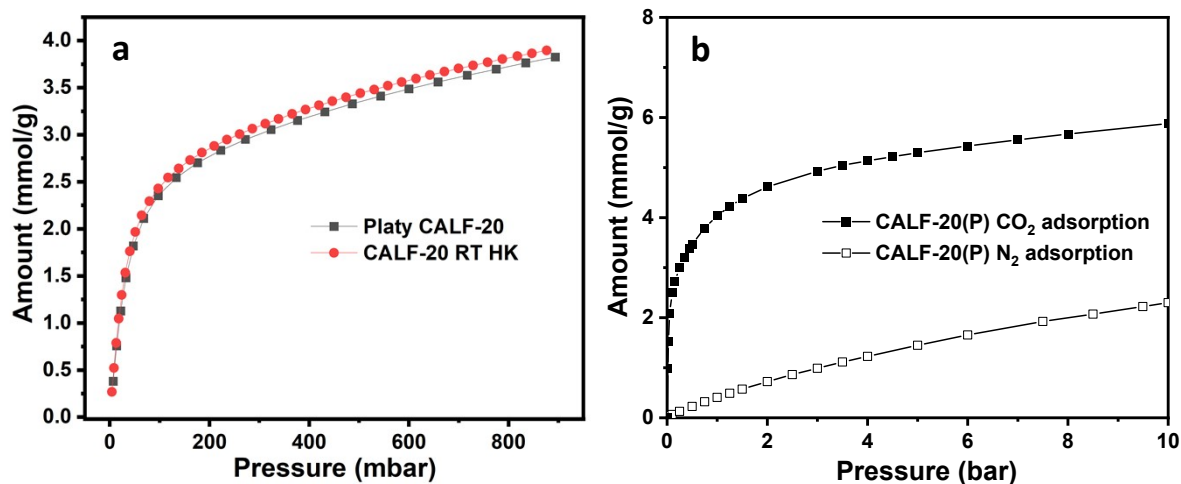
Figure S5. (a). CO_2 adsorption of platy CALF-20 compared to bulky CALF-20 synthesised under room temperature (named as CALF-20 RT HK); (b). N_2 and CO_2 isotherms at 298 K for CALF-20(P).
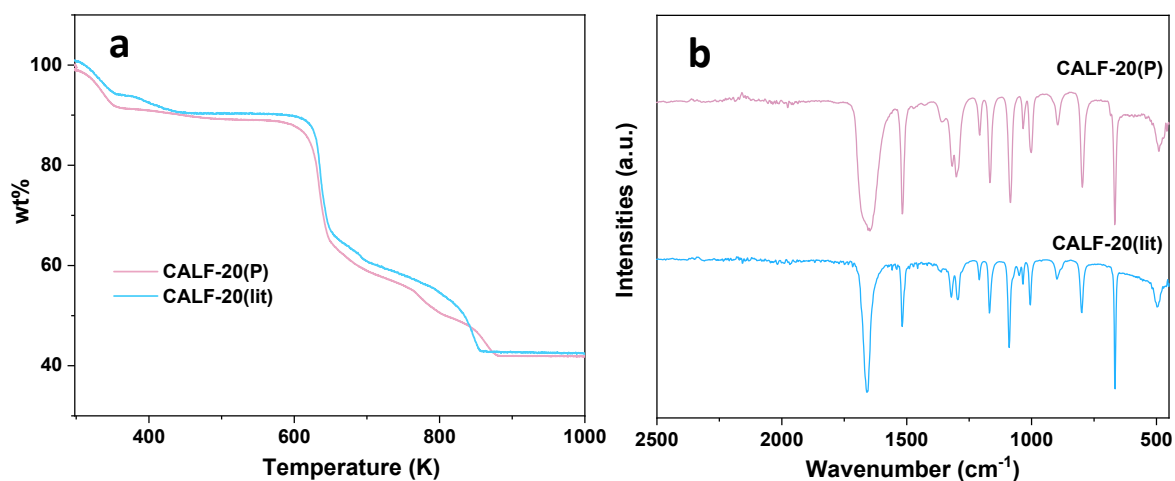

Figure S6. (a) TGA curve of CALF-20(P) compared to CALF-20 prepared via the literature method (CALF-20(lit)), and (b) IR spectra of CALF-20(P) and CALF-20(lit).
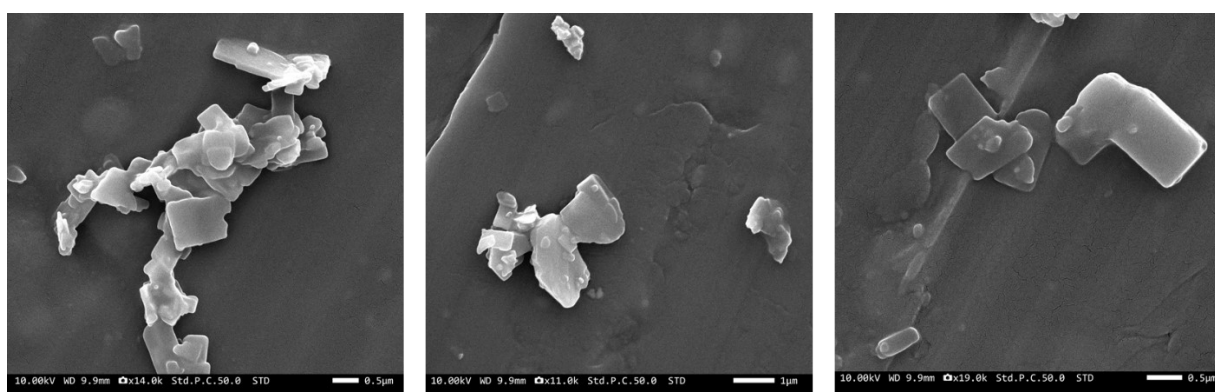

Figure S7. Representative SEM images of CALF-20(P) after sonication of as-prepared powder in methanol
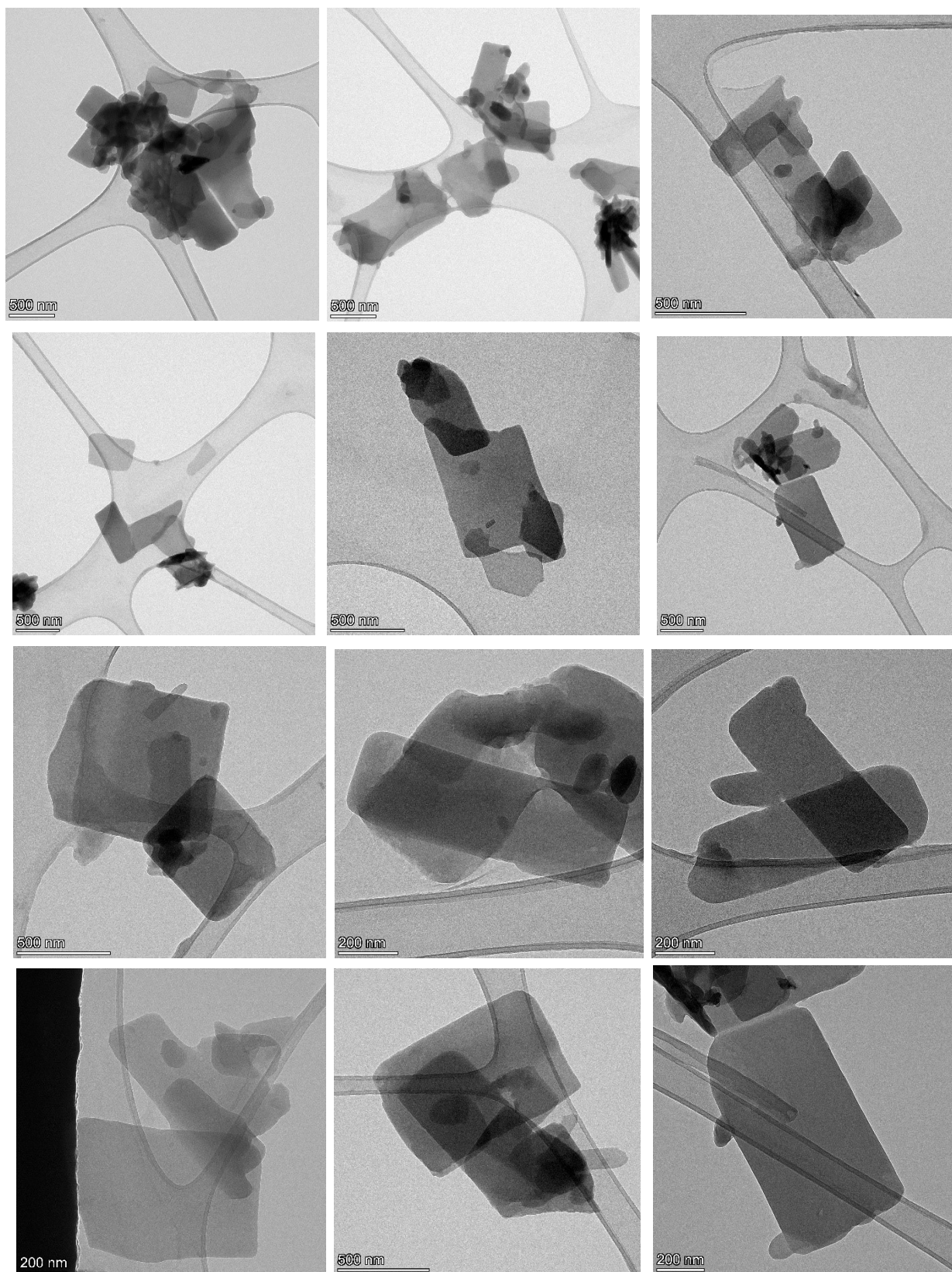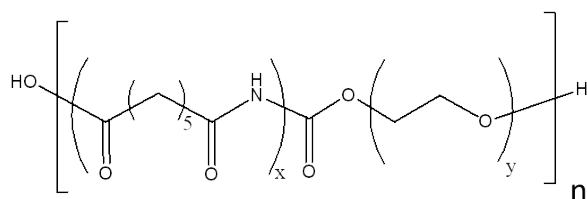
Figure S8. Typical TEM images of CALF-20(P) platelets after sonication of the as-prepared powder in methanol.

2. Preparation of PEBAX based MMMs and measurement of membrane performance

PEBAX MH1657 chemical structure (x=40, y=60)

Platy CALF-20 products [0.015 g (3%), 0.026 g (5%), 0.037 g (7%), 0.055 g (10%)] were suspended into a water/ethanol mixture (3.5g/7.9g). To obtain a homogeneous dispersion, the suspension was sonicated for 1 h. After sonication, 0.5 g PEBAX MH1657 was added into the suspension. The resultant mixture was transferred into a microwave reactor and stirred at 80 °C for 90 min to dissolve the polymer. The resulting solution was poured into a 5 cm glass petri dish. The membrane was allowed to form by slow solvent evaporation for 24 – 36 h.

The filler content in the above MMMs was calculated from:

$$W_{ZIF} = \frac{W_{ZIF}}{W_{ZIF} + W_{Polymer}}$$

(Eq. S1)

As a reference, membranes based on the neat polymers were also prepared by an identical procedure. The thickness of all membranes was around 50 μm, according to averaged measurements performed with a digital micrometre (Mitutoyo) at different locations on each membrane.

MMMs characterization

The crystalline structure of fabricated MMMs were investigated by PXRD in flat plate geometry, on a PANalytical Empyrean diffractometer with Cu $K_{\alpha 1}$ radiation and an X'celerator RTMS detector over a 2θ range of 3 – 40 °. The thermal behaviour of MMMs was measured by Netzsch Thermogravimetric Analyzer Jupiter STA449 with a heating rate of 10 °C min^{-1}. The membranes were examined with a JSM-IT100 (JEOL, Japan) operating at 10 kV. Before SEM analysis, the samples were fractured in liquid nitrogen and then sputtered with a layer of 12 nm gold to form a conductive surface.

Single permeation measurements

Single gas permeation measurements were carried out using a custom-built constant volume-variable pressure apparatus[6] using pure N_2 and CO_2 at 1.2 bar and 293 K.

The permeability is obtained from the evolution of pressure of the downstream side. The permeability coefficient, P, was determined from the slope of the pressure vs. time curve under the steady-state condition (Equation S3):

$$P = \frac{l\,V_{down}}{A\,P_{up}RT}\left[\left(\frac{dP_{down}}{dt}\right)_{ss}\right]$$

(Eq. S3)

Where l is the membrane thickness, A is the membrane area, V_{down} is the downstream volume, P_{up} is the upstream pressure, P_{down} is the downstream pressure, T is the temperature recorded during analysis and R is the gas constant.

The time lag, θ, was used to determine the diffusivity coefficient D (Equation S4).

$$D = \frac{l^2}{6\theta}$$

(Eq. S4)

The solubility coefficient, S, for the gas in the polymer was evaluated indirectly, assuming the validity of the diffusion-solution mechanism (Equation S5):

$$S = \frac{P}{D}$$

(Eq. S5)

The ideal selectivity between two gas species i and j is the ratio of the two single gas permeabilities (Equation S6).

$$\alpha_{ij} = \frac{P(i)}{P(j)}$$

(Eq. S6)

To predict the impact of filler morphology on membrane performance, the modified Maxwell equation is employed, as shown below:

$$P_{MMM} = P_p\left[1 + \frac{(1+G)\phi_d}{\left(\frac{P_d/P_c + G}{P_d/P_c - 1}\right) - \phi_d}\right]$$

(Eq. S7)

where the P_{MMM} is the gas permeability of the mixed matrix membranes, P_p is the gas permeability of the polymer matrix which can be obtained from the experiment, P_d is the gas permeability of the filler, Φ_d is the volume fraction of the filler; G is the geometric factor depending on the effect of the dispersion morphology.[7]

Mixed gas permeation measurements

Gas permeability measurements were performed with a mixed gas-continuous flow permeation cell designed in our laboratory.[8] Pure gases (CO_2 or N_2) were fed to the system with mass flow controllers (Bronkhorst Company, Netherlands), according the desired CO_2 concentration. The stream was

humidified (RH=50% and 90%) using a controlled evaporating and mixing system (Bronkhorst Control Evaporator Mixer W-202A-221-K). The total pressure of the humid feed and retentate streams were controlled by a back pressure controller (Bronkhorst Company, Netherlands) and the permeate stream was collected using a helium sweep gas with a controlled flow rate (5 Ncc/min, Bronkhorst Company, Netherlands). The permeation cell was placed in a heating cabinet (Carbolite PF030-230SN) in order to maintain a constant temperature (40 °C). All the tubing was heated with heater ropes in order to avoid any condensation in the rig.

The relative humidity and the gas concentration of the streams were measured using respectively a humidity sensor (developed in-house based on the Honeywell HIH4000 chip) and a mass spectrometer (Proline, AMETEK). The temperature of each stream was measured using a thermocouple (K insulated 1.5 mm thermocouple).

The temperature, the relative humidity and the gas composition of the permeate stream were recorded until the system equilibrium was reached (typically 2 – 3 h). The flow rates of the retentate and permeate were measured using mass flow meters (Bronkhorst Company, Netherlands), after passing through a water trap.

The permeability of each gas species passing through the membrane was calculated by Equation S8:

$$Perm(G) = \frac{e \times Flow^e \times X^P}{A \times (p^F - p^P)}$$

(Eq. S8)

Where e is the thickness of the membrane (cm), $Flow^P$ the permeate flowrate (cm^3 (STP)/s), X^P the mole fraction of the gas in the permeate stream, A the effective membrane area (cm^2), p^F and p^P the partial pressure of the gas in the feed and permeate stream respectively (cmHg).

A fresh membrane was used for each experimental run that consisted in firstly the measurement of the dry mixture, and secondly the wet mixture at the chosen water vapour activity. Between two runs, the rig was evacuated until the humidity sensor detected no water, approximately 10 h.

Table S2 Intrinsic properties of CALF-20 where the gas solubility is measured from gas adsorption, gas diffusivity is obtained according to previous literature[9] and gas permeability is the product of gas diffusivity and solubility according to Eq. S5.

MOF	CO_2 permeability (Barrer)	CO_2 diffusivity (cm^2/s)	CO_2 solubility (cm^3(STP)/(cm^3·cmHg))
CALF-20	713	1E-7	0.7

Table S3 CO_2 and N_2 uptake of CALF-20(P) at 1.2 bar and 298 K and the corresponding CO_2/N_2 selectivity.

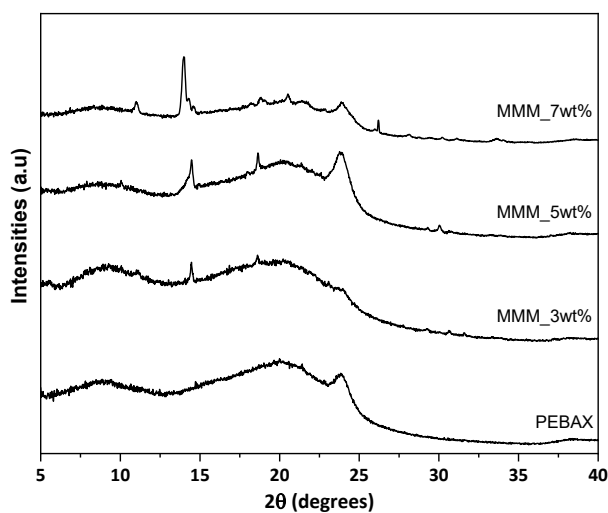| Sample	CALF-20(P)
CO_2 uptake (mmol g^{-1})	4.22
N_2 uptake (mmol g^{-1})	0.49
CO_2/N_2 selectivity	8.61

Figure S9. XRD patterns of MMMs incorporated platy CALF-20 at different loading compared to pure PEBAX membrane.
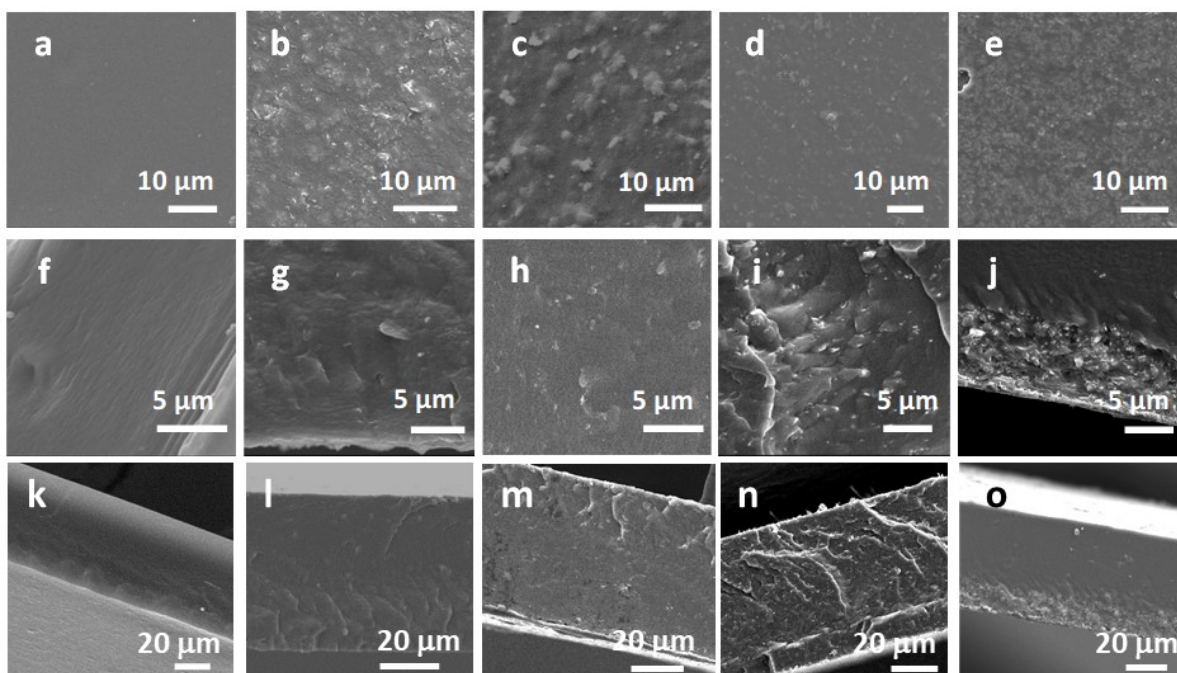
Figure S10. Surface (top row) and cross-section (bottom row) of the pure PEBAX 1657 membrane (a, f and k) and MMMs with 3 wt% (b, g and l), 5 wt% (c, h and m), 7 wt% (d, i and n) and 10 wt% (e, j and o).
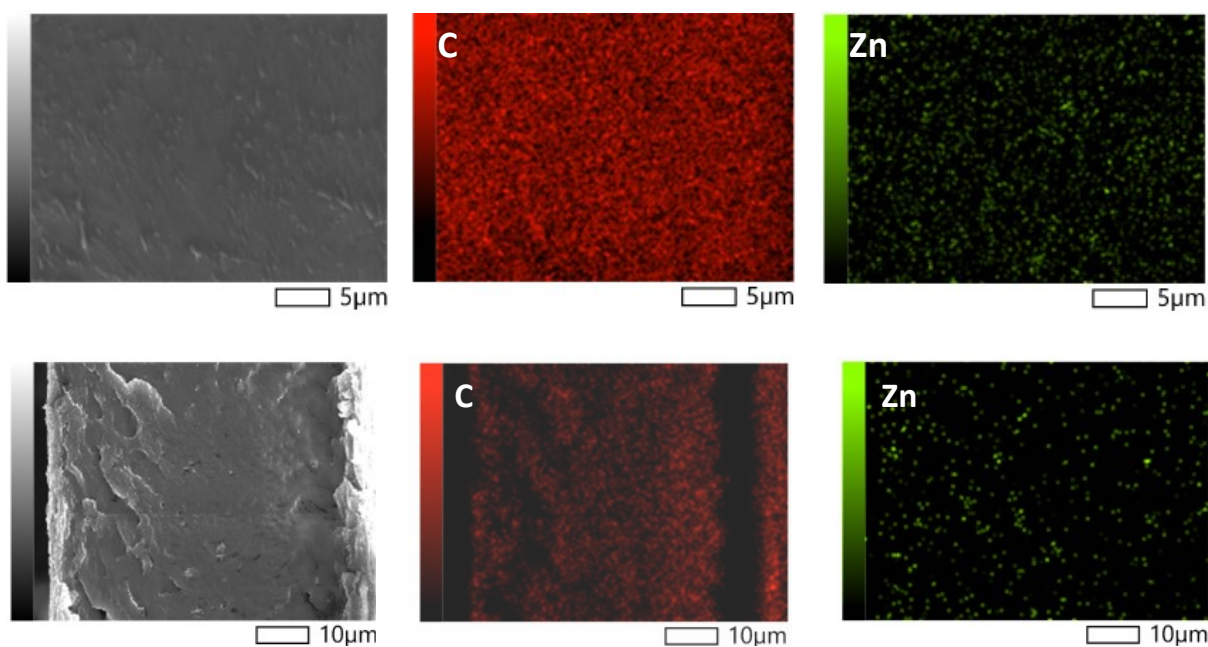

Figure S11. Elemental C and Zn mapping of the cross-section of MMM with 5 wt% CALF-20 plates, at two different scales. In the bottom images the full membrane is shown.
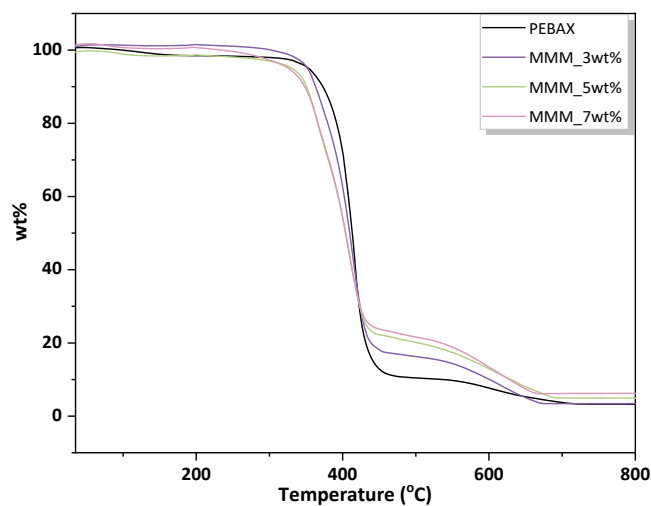
Figure S12. TGA curves of PEBAX-based MMMs containing CALF-20(P) at different loading compared to pure PEBAX membrane.
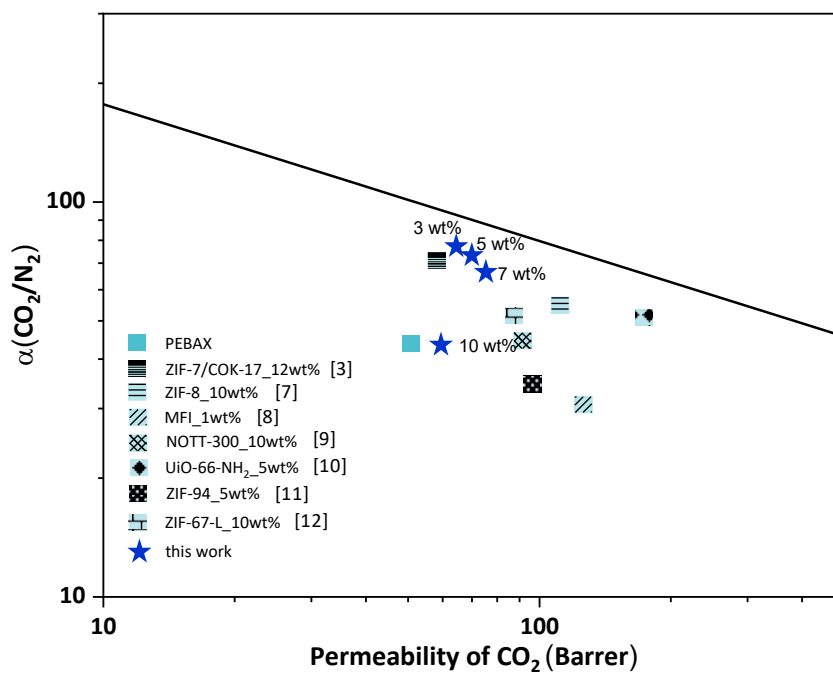

Figure S13. Robeson plot of membrane performance in this work compared to other PEBAX-based MMMs reported previously.[10-15] The 2008 Robeson upper bound is shown by the black line.
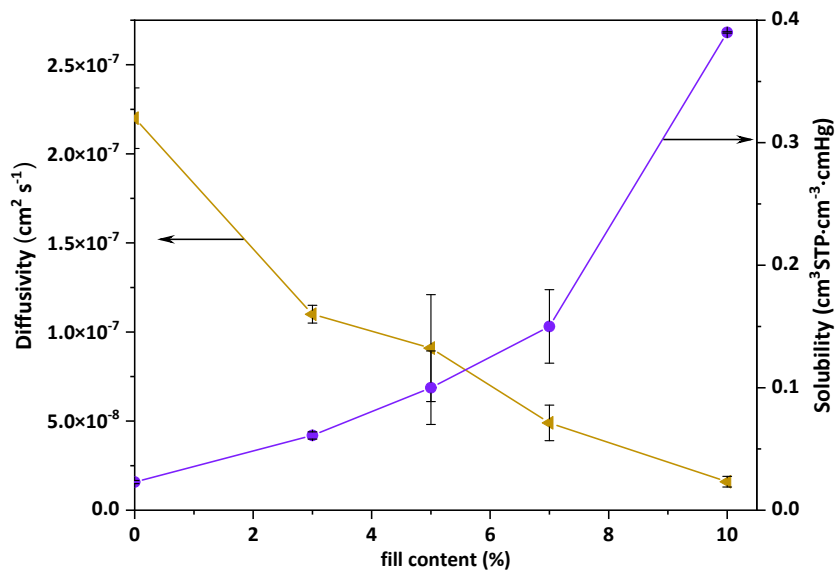
Figure S14. CO_2 diffusivity (in brown) and solubility (in blue) for the CALF-20_PEBAX_MMMs as a function of filler content.
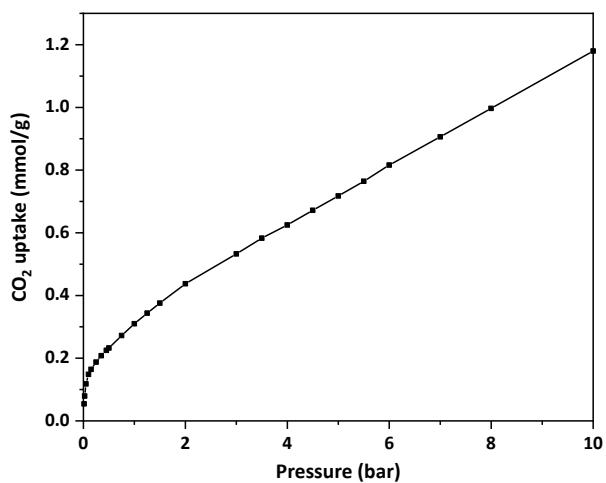

Figure S15. The CO_2 adsorption isotherm of MMM with 7 wt% CALF-20 at 298 K.
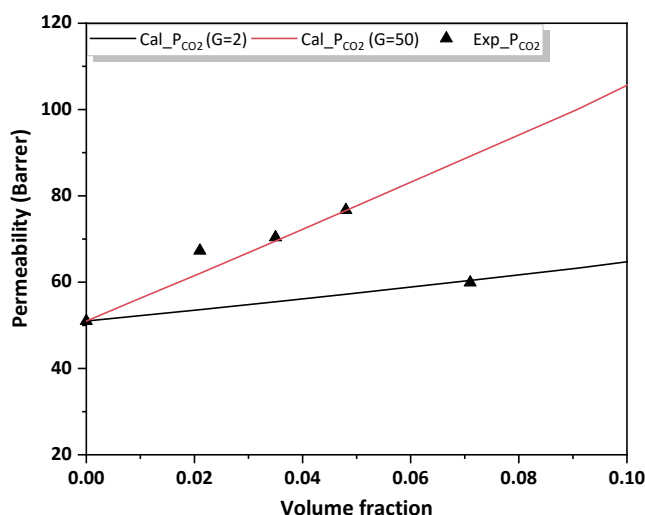
Figure S16. Comparison between the experimental CO_2 permeability and the theoretical data from modified Maxwell model: the experimental CO_2 permeability (solid triangle), and the predicted results for CO_2 permeability when incorporating spherical fillers (solid black line; G = 2) and platelet fillers (solid red line; G=50).

References

1. J.-B. Lin et al., A scalable metal-organic framework as a durable physisorbent for carbon dioxide capture. *Science,* **2021**, *374*, 1464–1469.

2. J. Taylor, R. Mah and G. Shimizu, Synthesis of zinc MOF materials, *US Patent,* **2022**, 11,230,562

3. W. Stählin and H. R. Oswald, The crystal structure of zinc hydroxide nitrate, $Zn_5(OH)_8(NO_3)_2 \cdot 2H_2O$, *Acta Cryst. B*, 1970, 26, 860-863.

4. S.-Q. Yang et al., Immobilization of the polar group into an ultramicroporous metal–organic framework enabling benchmark inverse selective CO_2/C_2H_2 separation with record C_2H_2 production. *J. Am. Chem. Soc.* **2023**, *145*, 13901-13911.

5. A. A Coelho, "TOPAS-Academic," can be found under: http://www.topas-academic.net/Technical_Reference.pdf, 2020.

6. Q. Jia, E. Lasseuguette, M. M. Lozinska, M.-C. Ferrari, and P. A. Wright, Hybrid Benzimidazole–Dichloroimidazole Zeolitic Imidazolate Frameworks Based on ZIF-7 and Their Application in Mixed Matrix Membranes for CO_2/N_2 Separation, *ACS Appl. Mater. Interfaces*, **2022**, *14*, 46615–46626.

7. Y. Eremin, A. Grekhov and A. Belogorlov, Percolation Effects in Mixed Matrix Membranes with Embedded Carbon Nanotubes. *Membranes,* **2022**, *12*, 1100.

8. B. Dhuiège, E. Lasseuguette, S. Brochier, M.-C. Ferrari and K. Missoum, Crosslinked Facilitated Transport Membranes Based on Carboxymethylated NFC and Amine-Based Fixed Carriers for Carbon Capture, Utilization, and Storage Applications. *Appl. Sci.* **2020**, *10*, 414.

9. M. Yann, D. Estelle, G. Maurin and P. L. Llewellyn, Abnormal CO_2 and H_2O Diffusion in CALF-20 (Zn) Metal-Organic Framework Angstropores. *ACS. Appl. Nano Mater.,* **2023**, *6*, 19963–19971.

10. W. Zheng et al., ZIF-8 nanoparticles with tunable size for enhanced CO_2 capture of Pebax based MMMs. *Sep. Purif. Technol.* **2019**, *214*, 111–119.

11. Q. Zhang, M. Zhou, X. Liu and B. Zhang, Pebax/two-dimensional MFI nanosheets mixed-matrix membranes for enhanced CO_2 separation. *J. Memb. Sci.,* **2021**, *636*, 119612.

12. N. Habib et al., Development of highly permeable and selective mixed matrix membranes based on Pebax®1657 and NOTT-300 for CO_2 capture. *Sep. Purif. Technol.,* **2020**, *234*, 116101.

13. P.-H. Tang et al., Carbon Dioxide Enrichment PEBAX/MOF Composite Membrane for CO_2 Separation. *Membranes,* **2021**, *11*, 404

14. M. R. Hasan, L. Paseta, M. Malankowska, C. Téllez and J. Coronas, Synthesis of ZIF-94 from Recycled Mother Liquors: Study of the Influence of Its Loading on Postcombustion CO_2 Capture with Pebax Based Mixed Matrix Membranes. *Adv. Sustain. Syst.,* **2022**, *6*, 2100317.

15. Q. Zhao, S. Lian and R. Li et al., Fabricating Leaf-like hierarchical ZIF-67 as Intra-Mixed matrix membrane microarchitecture for efficient intensification of CO_2 separation. *Sep. Purif. Technol.,* **2023**, *305,* 122460.